2011 50th IEEE Conference on Decision and Control and
European Control Conference (CDC-ECC)
Orlando, FL, USA, December 12-15, 2011

Collision Avoidance Maneuver Design Based on Equidistance Interpolation

Yongqiang Qi, Yingmin Jia, Junping Du and Fashan Yu

Abstract— **This paper deals with the active collision avoidance maneuver for the chaser along the specified trajectory, and presents a maneuver approach with constant thrust. Using the 3D stereo vision measurement, The relative position parameters of the target spacecraft for analyzing the collision possibility are obtained by using the vision measurement and the target maneuver positions are calculated through the equidistance interpolation method. The working times of thrusters in three axes can be respectively computed by the time series analysis method. In particular, the perturbation and fuel consumption are addressed during the computation of working time. Furthermore, the acceleration sequences and the corresponding working time series can be employed to determine a switching control law for the active collision avoidance maneuver. The simulation results show that the switch control law can effectively guarantee the chaser moving along the specified trajectory.**

Index Terms— **Constant thrust; Vision measurement; Switch control law; The specified trajectory; Equidistance interpolation.**

I. Introduction

The problem of collision avoidance impulsive maneuvers in the process of rendezvous and docking has been under intensive investigation for several decades. In actual practice, however, maneuvers during rendezvous and docking operations cannot normally be considered as impulsive maneuvers because there exist long thrust arcs. Therefore, the impulse assumption does not hold any more. To overcome this problem, a novel active collision avoidance maneuver under constant thrust is proposed in this work.

The most common method to deal with the collision avoidance between two spacecrafts is to calculate the probability of collision firstly, then carry out active collision avoidance maneuver if there is the possibility of collision [1], [2]. However, due to the relative velocity is small in the rendezvous and docking stage, the calculation of collision probability is difficult to be linearized. Therefore, active collision avoidance maneuver in this paper is carried out according to the possibility of collision which is calculated based on the relative position and the relative velocity between the chaser and the target spacecraft.

Various types of safeties have been considered in the design of collision avoidance spacecraft trajectories [2]–[9]. Richards et al studied collision and plume avoidance to deal with spacecraft trajectory planning by using mixed integer linear programming [2]. Jacobsen et al presented a method for planning of safe Kinematic trajectories for free flying robots approaching an uncontrolled spinning satellite [6]. Methods proposed in Ref. [6] develop the safety circle method in which a nearby orbit with a relative invariant trajectory is established that allows safe long-term observation before docking. However, this approach is not fuel optimized and does not propose a specific collision avoidance maneuvers route.

The purpose of this paper is to analyze the collision possibility between the chaser and target spacecraft and to enact active collision avoidance constant thrust maneuver along the specified trajectory. The specified trajectory is given according to the initial relative position and the terminal target position of the chaser, at the same time the size and the direction of the initial relative velocity and the acceleration are also taken into account. First of all, the relative position parameters of the spacecrafts are obtained by using vision measurement. Next, the definition of the spherical security zones and the criterions of the collision possibility are presented. Then, to ensure the chaser moving along the specified trajectory, the equidistance interpolation method is used by dividing the entire process of the active collision avoidance maneuver into equidistance arcs. At last, the actual working times of the thrusters in three axes can be respectively computed by using the time series analysis method. Moveover, the switch control laws in the three axes for active collision avoidance constant thrust maneuvers are designed based on the actual working time series and the corresponding accelerations. The simulation results show that the constant thrust maneuver can effectively guarantee the chaser maneuvering along the specified trajectory.

II. Vision Algorithm for Position Determination

Two cameras C_1 and C_2 which have the same focal lengths and the internal parameters are installed in the chaser. Camera coordinate system is established as shown in Figure 1. O_{c_1} and O_{c_2} are the optical centers of the cameras C_1 and C_2, respectively. X_{c_1} and X_{c_2} are the optical axes of the cameras C_1 and C_2, respectively. X_{c_1} is parallel to X_{c_2}, and

This work was supported by the NSFC (60727002, 60774003, 60921001, 90916024), the MOE (20030006003), the COSTIND (A2120061303) and the National 973 Program (2005CB321902).

Yongqiang Qi is with the Seventh Research Division and the Department of Systems and Control, Beihang University (BUAA), Beijing 100191, China (e-mail: qiyongqiang3@163.com).

Yingmin Jia is with the Seventh Research Division and the Department of Systems and Control, Beihang University (BUAA), Beijing 100191, China. He is also with the Key Laboratory of Mathematics, Informatics and Behavioral Semantics (LMIB), Ministry of Education, SMSS, Beihang University (BUAA), Beijing 100191, China (e-mail: ymjia@buaa.edu.cn).

Junping Du is with Beijing Key Laboratory of Intelligent Telecommunications Software and Multimedia, School of Computer Science and Technology, Beijing University of Posts and Telecommunications, Beijing 100876, China (e-mail: junpingdu@126.com)

Fashan Yu is with School of Electrical Engineering and Automation, Henan Polytechnic University, Jiaozuo 454000, Henan, China (e-mail: yufs@hpu.edu.cn)

Y_{c_1} coincides with Y_{c_2}, where The optical parallax between O_{c_1} and O_{c_2} is L. P is any point on the target spacecraft, P_1 and P_2 are the projection points of the P on the image planes of the cameras C_1 and C_2, respectively. therefore, P is the intersection of $O_{c_1}P$ and $O_{c_2}P$.

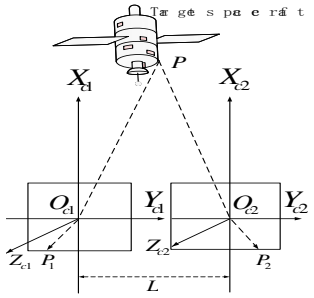

Figure 1. Model of binocular vision.

Further assume that the cameras have been calibrated and their projection matrices are M_1 and M_2 [10]. The following results can be obtained by coordinate transformation

$$X_{c_i}\begin{pmatrix} x_1 \\ y_1 \\ 1 \end{pmatrix} = M_i \begin{pmatrix} X \\ Y \\ Z \\ 1 \end{pmatrix} \tag{1}$$

$$M_i = \begin{pmatrix} m_{11}^i & m_{12}^i & m_{13}^i & m_{14}^i \\ m_{21}^i & m_{22}^i & m_{23}^i & m_{24}^i \\ m_{31}^i & m_{32}^i & m_{33}^i & m_{34}^i \end{pmatrix}, \ i = 1, 2 \tag{2}$$

where $(x_1, y_1, 1)^T$ and $(x_2, y_2, 1)^T$ are homogeneous coordinates of P_1 and P_2 in the cameras C_1 and C_2, respectively. $(X, Y, Z, 1)^T$ is the homogeneous coordinate of P in the reference coordinate system, that is to say, X, Y and Z are the 3D position coordinates of the real point P. Therefore, X_{c_1} and X_{c_2} can be removed by combining (1) and (2),

$$A(X, Y, Z)^T = B \tag{3}$$

$$A = \begin{pmatrix} x_1 m_{31}^1 - m_{11}^1 & x_1 m_{32}^1 - m_{12}^1 & x_1 m_{33}^1 - m_{13}^1 \\ y_1 m_{31}^1 - m_{21}^1 & y_1 m_{32}^1 - m_{22}^1 & y_1 m_{33}^1 - m_{23}^1 \\ x_2 m_{31}^2 - m_{11}^2 & x_2 m_{32}^2 - m_{12}^2 & x_2 m_{33}^2 - m_{13}^2 \\ y_2 m_{31}^2 - m_{21}^2 & y_2 m_{32}^2 - m_{22}^2 & y_2 m_{33}^2 - m_{23}^2 \end{pmatrix} \tag{4}$$

$$B = \begin{pmatrix} m_{14}^1 - x_1 m_{34}^1 \\ m_{24}^1 - y_1 m_{34}^1 \\ m_{14}^2 - x_2 m_{34}^2 \\ m_{24}^2 - y_2 m_{34}^2 \end{pmatrix} \tag{5}$$

The least-square solution of P in the reference coordinate system as follow [11].

$$(X, Y, Z)^T = (A^T A)^{-1} A^T B \tag{6}$$

Assume that the virtual optical center of the cameras C_1 and C_2 is the midpoint of the line segment $O_{C_1}O_{C_2}$ and defined as O_C, and the virtual optical axis is parallel to $O_{c_i}X_{c_i}(i = 1, 2)$, the other two axes are coincide with $O_{c_i}Y_{c_i}(i = 1, 2)$ and parallel to $O_{c_i}Z_{c_i}(i = 1, 2)$, respectively. According to the definition of the coordinate system (Geller, 2006),

$$X = \frac{fL}{(x_2 - x_1)dy}, \ Y = \frac{x_1 - x_0}{(x_2 - x_1)}L, \ Z = \frac{(y_1 - y_0)dz}{(x_1 - x_2)dy}L. \tag{7}$$

where f is the focal length of the camera, (x_0, y_0) is the projection point of the P on the image plane from the virtual optical center O_C. Therefore, the following results can be obtained according to vision measurement errors

$$\begin{aligned} dX &= \frac{\partial X}{\partial x_1}dx_1 + \frac{\partial X}{\partial x_2}dx_2 \\ &= \frac{fL}{(x_2 - x_1)^2 dy}dx_1 - \frac{fL}{(x_2 - x_1)^2 dy}dx_2 \end{aligned} \tag{8}$$

$$\begin{aligned} dY &= \frac{\partial Y}{\partial x_1}dx_1 + \frac{\partial Y}{\partial x_2}dx_2 \\ &= \frac{(x_2 - x_0)L}{(x_2 - x_1)^2}dx_1 - \frac{(x_1 - x_0)L}{(x_2 - x_1)^2}dx_2 \end{aligned} \tag{9}$$

$$\begin{aligned} dZ &= \frac{\partial Z}{\partial x_1}dx_1 + \frac{\partial Z}{\partial x_2}dx_2 + \frac{\partial Z}{\partial x_2}dy_1 \\ &= \frac{(y_1 - y_0)L}{(x_2 - x_1)^2}dx_1 - \frac{(y_1 - y_0)L}{(x_2 - x_1)^2}dx_2 + \frac{L}{x_2 - x_1}dy_1 \end{aligned} \tag{10}$$

where the independent parameters dx_1, dx_2, dy_1, dy_2 are the pixel position measurement errors of the cameras C_1 and C_2

III. The Criterion for Judging Collision Possibility

The chaser's spherical security zone S_C and target spacecraft's security zone S_T as shown in Figure 2. The security zone S_C is defined by the following steps.

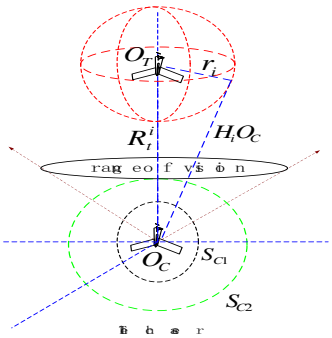

Figure 2. Security zones of the chaser and the target.

Step 1: The center of spherical security zone O_C is the middle point of O_{C_1} and O_{C_2}. The maximum distance from all points within the cone-shaped range of vision to O_C is recorded as R_1. The first layer spherical security zone is defined as S_{C1} whose radius is R_1. Step 2: The second layer spherical security zone of the chaser is S_{C2} whose radius is R_2 which is the maximum distance from all points in the chaser to O_C.

The security zone S_T is given by the following steps. Step 1: The center point of spherical security zone is defined as O_T which is the center point of the target spacecraft. The distance from O_T to O_C at the ith target positions

marked $R_t^i (i = 1, 2, ...N)$. The longest line segments from all edge points of the target spacecraft to O_C at the N target maneuver positions are recorded as $H_iO_C, i \in \{1, 2, ...N\}$. The angles between H_iO_C and O_TO_C are recorded as $\theta_i, i \in \{1, 2, ...N\}$. Step 2: The radius R_t of the spherical security zone S_T by using law of cosines as follows.

$$r_i = [(R_t^i)^2 + (H_iO_C)^2 - 2R_t^i(H_iO_C)\cos\theta_i]^{\frac{1}{2}} \tag{11}$$

The angle between O_CO_T and the direction of relative velocity is recorded as α. When $\alpha = 0$, safe distance and the corresponding minimum time are defined as d_{i1} and t_{i1}. If the distance $|O_CO_T|$ and the relative velocity v_{i1} meet the following conditions:

$$|O_CO_T| - r_i - R_2 > d_{i1} \tag{12}$$
$$|O_CO_T| - r_i - R_2 \gg V_{i1}t_{i1} \tag{13}$$

there is no possibility of collision. If the distance $|O_CO_T|$ and the relative velocity v_{i1} meet the following conditions

$$|O_CO_T| - r_i - R_2 < d_{i1} < |O_CO_T| - R - R_1 \tag{14}$$
$$|O_CO_T| - r_i - R_1 > v_{i1}t_{i1} \tag{15}$$

the chaser should carry out active collision avoidance maneuver within the time $\frac{|O_CO_T|-r_i-R_1}{v_{i1}} - t_{i1}$.

In case of $\alpha \neq 0$, the minimum safe distance and the corresponding minimum time are defined as d_{i2} and t_{i2}. If the distance $|O_CO_T|$ and the relative velocity v_{i2} meet the following conditions

$$|O_CO_T| - r_i - R_2 \gg d_2 \tag{16}$$
$$|O_CO_T|\sin\alpha - r_i - R_2 \gg d_2 \tag{17}$$

there is no possibility of collision. If the distance R_t^i and the relative velocity V_{i2} meet the following conditions, there is a possibility of collision,

$$R_t^i \sin\alpha_i - r_i - R_2 < d_{i2} < R_t^i \sin\alpha_i - r_i - R_1 \tag{18}$$
$$R_t^i \cos\alpha_i - [(r_i + d_{i2} + R_2)^2 - (R_t^i)^2 \sin^2\alpha_i]^{\frac{1}{2}} > V_i t_{i2} \tag{19}$$

the chaser should carry out active collision avoidance maneuver to arrive at one point outside of the hemispherical with radius $r_i + d_{i1} + R_2$.

IV. Switching Control Laws for Collision Avoidance Maneuver

The target spacecraft is assumed as a rigid body and in circular orbits. The relative motion can be described by Clohessy-Wiltshire equations. The origin of coordinate is O_T, the $x - axis$ is along the opposite direction of target velocity, the $y - axis$ is along the radius direction from the centroid of earth to the centroid of target spacecraft and the $z - axis$ satisfies the right-handed coordinate system.

$$\ddot{x} - 2\omega\dot{y} = a_x + a_x^p \tag{20}$$
$$\ddot{y} + 2\omega\dot{x} - 3\omega^2 y = a_y + a_y^p \tag{21}$$
$$\ddot{z} + \omega^2 z = a_z + a_z^p \tag{22}$$

where ω represents the mean angular velocity of the target spacecraft. a_x, a_y and a_z represent the thrust accelerations of the chaser. a_x^p, a_y^p and a_z^p represent the sums of perturbation, and nonlinear factors. Suppose a_x^p, a_y^p and a_z^p satisfy the conditions:

$$a_x^p \approx \eta_x a_x, \quad a_y^p \approx \eta_y a_y, \quad a_z^p \approx \eta_z a_z \tag{23}$$

η_x, η_y, η_z change very little during active collision avoidance maneuver. Therefore, a_x, a_y, a_z can be seen as only relevant to the thrusts and the mass of the chaser.

$$a_i = \frac{F_i}{[m_0 - (\dot{m}_x t_x + \dot{m}_y t_y + \dot{m}_z t_z)]}. \quad i = x, y, z \tag{24}$$

where F_x, F_y, F_z represent the vacuum thrusts of the chaser in three axes. m_0 represents the initial mass of the chaser at the beginning of maneuver. $\dot{m}_x, \dot{m}_y, \dot{m}_z$ represent fuel consumption per second of the thrusters. t_x, t_y, t_z represent the working times of thrusters in their directions. Polynomial approximate expression of the Eq.(24) as follows:

$$a_i = F_i \sum_{j=0}^{n} \lambda_j t^j. \quad i = x, y, z \tag{25}$$

where λ_j are polynomial coefficients, t is the actual running time of the chaser and $t_i \leq t$ (i=x, y, z). Then the original system can be transformed into the form as follows.

$$\ddot{x} - 2\omega\dot{y} = (1 + \eta_x)F_x \sum_{j=0}^{n} \lambda_j t^j \tag{26}$$
$$\ddot{y} + 2\omega\dot{x} - 3\omega^2 y = (1 + \eta_y)F_y \sum_{j=0}^{n} \lambda_j t^j \tag{27}$$
$$\ddot{z} + \omega^2 z = (1 + \eta_z)F_z \sum_{j=0}^{n} \lambda_j t^j \tag{28}$$

The specified trajectory for active collision avoidance maneuver as shown in Figure 3.

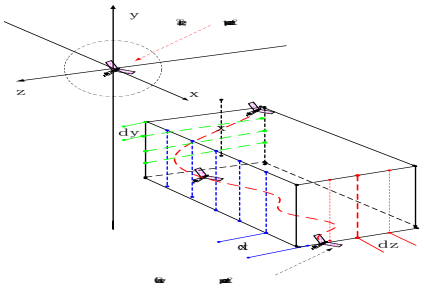

Figure 3: The specified trajectory.

$$\begin{cases} f(x, y, z) = 0 \\ g(x, y, z) = 0 \end{cases} \tag{29}$$

It is obvious that the specified trajectory is just in a cube $\Delta_x \times \Delta_y \times \Delta_z$ and can be divided into N equidistance arcs sequences in three axes, respectively. The length of equidistance arcs in three axes are Δxi, Δyi and $\Delta zi, i \in \{1, 2, ...N\}$. The current maneuver position and the next target maneuver position are in different side of surfaces

$(f(x,y,z)=0,\ g(x,y,z)=0)$. Therefore, the differential variables δ_f, δ_g and $f(x,y,z)$, $g(x,y,z)$ should have opposite algebraic signs.

$$\begin{cases} f(x,y,z)\cdot\delta_f \le 0 \\ g(x,y,z)\cdot\delta_g \le 0 \end{cases} \tag{30}$$

$$\delta_f = gradf\cdot(K_x^i\Delta xi, K_y^i\Delta yi, K_z^i\Delta zi) \tag{31}$$

$$\delta_g = gradg\cdot(K_x^i\Delta xi, K_y^i\Delta yi, K_z^i\Delta zi) \tag{32}$$

$$|K_x^i|+|K_y^i|+|K_z^i|\ge 1 \tag{33}$$

The equidistance arcs should parallel to the tangent of the specified trajectory to the maximum extent

$$\{(\tau_x^i,\tau_y^i,\tau_z^i)\cdot(K_x^i\Delta xi, K_y^i\Delta yi, K_z^i\Delta zi)\} \tag{34}$$

where $(\tau_x^i,\tau_z^i,\tau_z^i)$ is the tangent of the specified trajectory in the ith target maneuver position. According to Eqs.(30)(34) all the target maneuver positions can be obtained. The next maneuver target position is the current position add on increment of coordinate $(K_x^i\Delta xi, K_y^i\Delta yi, K_z^i\Delta zi)$.

Taking the working time of thruster in the ith arc in the $x-axis$ as an illustration: T_x^i is the maneuver time and t_x^i is the thruster working time. N_{xi}^a is the number of the accelerating time intervals $(t_{ax}^i)_j$, N_{xi}^c is the number of the decelerating time intervals $(t_{cx}^i)_j$, N_{xi}^b is the number of the zero-thrust time intervals $(t_{bx}^i)_j$ as shown in Figure 4.

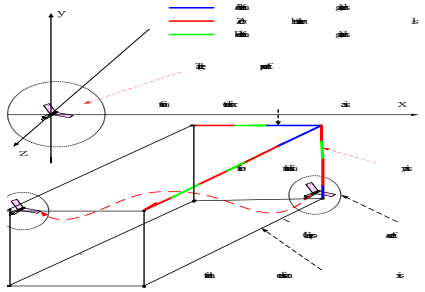

Figure 4: The change of time intervals in three axes.

$$T_m^i = \sum_{j=1}^{N_{mi}^a}(t_{am}^i)_j + \sum_{j=1}^{N_{mi}^b}(t_{am}^i)_j + \sum_{j=1}^{N_{mi}^c}(t_{cm}^i)_j \tag{35}$$

$$t_m^i = \sum_{j=1}^{N_{mi}^a}(t_{am}^i)_j + \sum_{j=1}^{N_{mi}^c}(t_{cm}^i)_j, m\in\{x,y,z\} \tag{36}$$

The working time time intervals of thrusters in the ith arc are calculated in two steps as follows.

(1) According to Eqs.(20)(21) the following results can be obtained.

$$\begin{aligned} x_i + K_x^i\Delta xi = {} & -2(v_{y0i}-\beta_1)\cos\omega T_x^i + \sum_{j=2}^{6}[2\omega\frac{1}{j}\beta_{j-1} \\ & + (1+\eta_x)F_x\frac{1}{(j-1)j}\lambda_{j-2}^i](T_x^i)^j + (v_{x0}-2y_{0i}\omega)T_x^i \\ & + x_{0i} + 2v_{y0i} - 2\beta_1 + 2y_{0i}\sin\omega T_x^i \end{aligned} \tag{37}$$

$$\begin{aligned} v_x = {} & 2\omega(v_{y0i}-\beta_1)\sin\omega T_x^i + 2\omega y_{oi}\cos\omega T_x^i + \sum_{j=1}^{5}[2\omega\beta_j \\ & + j(1+\eta_x)F_x\lambda_{j-1}](T_x^i)^j + v_{x0i} - 2\omega y_{0i} \end{aligned} \tag{38}$$

$$\begin{aligned} y_i + K_y^i\Delta yi = {} & y_{0i}cos\omega T_y^i + \frac{(v_{y0i}-\beta_1)}{\omega}\sin\omega T_y^i \\ & + \sum_{j=1}^{5}\beta_j(T_y^i)^j \end{aligned} \tag{39}$$

$$\begin{aligned} v_y = {} & (v_{y0i}-\beta_1)\cos\omega T_y^i - \omega y_{0i}\sin\omega T_y^i \\ & + \sum_{j=0}^{4}(j+1)\beta_{j+1}(T_y^i)^j \end{aligned} \tag{40}$$

$$\begin{aligned} \beta_{1i} = {} & -\frac{2(1+\eta_x)F_x}{\omega}\lambda_{0i} + \frac{(1+\eta_y)F_y}{\omega^2}\lambda_{1i} + \frac{4(1+\eta_x)F_x}{\omega^3}\lambda_{2i} \\ & - \frac{6(1+\eta_y)F_y}{\omega^4}\lambda_{3i} - \frac{48(1+\eta_x)F_x}{\omega^5}\lambda_{4i} \end{aligned} \tag{41}$$

$$\begin{aligned} \beta_{2i} = {} & -\frac{(1+\eta_x)F_x}{\omega}\lambda_{1i} + \frac{(1+\eta_y)F_y}{\omega^2}\lambda_{2i} + \frac{6(1+\eta_x)F_x}{\omega^3}\lambda_{3i} \\ & - \frac{12(1+\eta_y)F_y}{\omega^4}\lambda_{4i} \end{aligned} \tag{42}$$

where $\beta_{1i},...,\beta_{2i}$ are polynomial coefficients in the ith thrust arc. (x_{0i},y_{0i}) and (v_{x0i},v_{y0i}) are the initial relative position and the initial relative velocity of the chaser in the $x-axis$ and the $y-axis$ at the beginning of the ith thrust arc, respectively. According to Eqs.(41)-(45), $\beta_{1i},...\beta_{5i}$ can be expressed by $\lambda_{1i},...,\lambda_{4i}$, where $\lambda_{1i},...,\lambda_{4i}$ are polynomial coefficients in the ith thrust arc. $\lambda_{0i}=\frac{1}{m_i}$ represents the initial mass of the chaser at the beginning of the ith thrust arc.

Then consider the maneuver in the direction of the $z-axis$, the following results can be obtained the following two results are obtained according to Eq.(22)

$$\begin{aligned} z_i + K_x^i\Delta zi = {} & [\frac{v_{z0i}}{\omega} - (1+\eta_z)(\frac{F_z}{\omega^3}\lambda_{1i} - \frac{6F_z}{\omega^5}\lambda_{3i})]\sin\omega T_z^i \\ & + [z_{0i} - (1+\eta_z)(\frac{F_z}{\omega^2}\lambda_{0i} - \frac{2F_z}{\omega^4}\lambda_{2i} + \frac{24F_z}{\omega^6}\lambda_{4i})]\cos\omega T_z^i \\ & + (1+\eta_z)[(\frac{F_z}{\omega^2}\lambda_{0i} - \frac{2F_z}{\omega^4}\lambda_{2i} + \frac{24F_z}{\omega^6}\lambda_{4i}) + (\frac{F_z}{\omega^2}\lambda_{1i} \\ & - \frac{6F_z}{\omega^4}\lambda_{3i})T_z^i + (\frac{F_z}{\omega^2}\lambda_{2i} - \frac{12F_z}{\omega^4}\lambda_{4i})(T_z^i)^2 \\ & + \frac{F_z}{\omega^2}\lambda_{3i}(T_z^i)^3 + \frac{F_z}{\omega^2}\lambda_{4i}(T_z^i)^4] \end{aligned} \tag{43}$$

$$\begin{aligned} v_{zi} = {} & [v_{z0i} - (1+\eta_z)(\frac{F_z}{\omega^2}\lambda_{1i} - \frac{6F_z}{\omega^4}\lambda_{3i})]\cos\omega T_z^i \\ & - [\omega z_{0i} - (1+\eta_z)(\frac{F_z}{\omega}\lambda_{0i} - \frac{2F_z}{\omega^3}\lambda_{2i} - \frac{2F_z}{\omega^3}\lambda_{2i} \\ & + \frac{24F_z}{\omega^5}\lambda_{4i})]\sin\omega T_z^i + (1+\eta_z)[(\frac{F_z}{\omega^2}\lambda_{1i} - \frac{6F_z}{\omega^4}\lambda_{3i}) \\ & + 2(\frac{F_z}{\omega^2}\lambda_{2i} - \frac{12F_z}{\omega^4}\lambda_{4i})T_z^i + 3\frac{F_z}{\omega^2}\lambda_{3i}(T_z^i)^2 \\ & + 4\frac{F_z}{\omega^2}\lambda_{4i}(T_z^i)^3] \end{aligned} \tag{44}$$

where z_{0i} and v_{z0i} are the initial relative position and the initial relative velocity of the chaser in the $z-axis$ at the beginning of the ith thrust arc. Because the ith target maneuver position (x_i,y_i,z_i) and ith target maneuver velocity

(v_{xi}, v_{yi}, v_{zi}) are known, so the $i+1$th target maneuver position is $(x_i + K_x^i \Delta xi, y_i + K_y^i \Delta yi, z_i + K_z^i \Delta zi)$. Therefore, polynomial coefficients $\lambda_{1i}, ..., \lambda_{4i}$ can be obtained according to Eqs.(37)-(40),(46),(47).

(2)According to Eq.(25), the thrusters working times t_x^i, t_y^i, t_z^i in the ith arc can be calculated as follows

$$\frac{1}{m_i - (\dot{m}_x t_x^i + \dot{m}_y t_y^i + \dot{m}_z t_z^i)} = \sum_{j=0}^{4} \lambda_{ji} (\max\{t_x^i, t_y^i, t_z^i\})^j \tag{45}$$

T_x^i, T_y^i, T_z^i are divided into N_x^i, N_y^i, N_z^i equal time intervals in three axes, respectively. Taking T_x^i and t_x^i as an example

$$T_x^i = [T_{x1}^i, ..., T_{xN_x^i}^i]; \quad t_x^i = [t_{x1}^i, ..., t_{xN_x^i}^i] \tag{46}$$

if $t_{x1}^i = max\{t_{x1}^i, t_{y1}^i, t_{z1}^i\}$, then

$$\frac{1}{m_i - (\dot{m}_x t_{x1}^i + \dot{m}_y t_{y1}^i + \dot{m}_z t_{x1}^i)} = \sum_{j=0}^{4} \lambda_{ji} (t_{x1}^i)^j \tag{47}$$

t_{x1}^i, $t_{y1}^i$and t_{z1}^i can be calculated. If T_{x2}^i meets the following conditions: $t_{x2}^i = min\{t_{x2}^i, t_{y2}^i, t_{z2}^i\}$ and $t_{x1}^i + t_{x2}^i = max\{t_{x1}^i + t_{x2}^i, t_{y1}^i + t_{y2}^i, t_{z1}^i + t_{z2}^i\}$, then

$$\frac{1}{m_i - (\dot{m}_x t_{x1}^i + \dot{m}_y t_{y1}^i + \dot{m}_z t_{z1}^i) - (\dot{m}_x t_{x2}^i + \dot{m}_y t_{y2}^i + \dot{m}_z t_{x2}^i)} = \sum_{j=0}^{4} \lambda_{ji} (t_{x1}^i + t_{x2}^i)^j \tag{48}$$

$t_{x2}^i, t_{y2}^i, t_{z2}^i$ can be calculated. Then $\{t_{y1}^i, t_{y2}^i, ..., t_{yN_y^i}^i\}$ and $\{t_{z1}^i, t_{z2}^i, ..., t_{zN_z^i}^i\}$ can be deduced by analogy. If $t_{xk}^i = 0, k \in (1, 2, ...N_x^i)$, then t_{xk}^i belongs to zero-thrust intervals; If $t_{xk}^i \neq 0, k \in (1, 2, ...N_x^i)$ and meets the following conditions.

$$|v_{x(i-1)}| < |v_{xi}|, \quad v_{x(i-1)} v_{xi} \geq 0 \tag{49}$$

$v_{x(i-1)} > 0$, then t_{xk}^i belongs to accelerating intervals and the direction of F_x is along the positive direction of the x-axis; $v_{x(i-1)} \leq 0$, then t_{xk}^i belongs to accelerating intervals but the direction of F_x is along the negative direction of the x-axis. If $t_{xk}^i \neq 0, k \in (1, 2, ...N_x^i)$ and meets the following conditions.

$$|v_{x(i-1)}| > |v_{xi}|, \quad v_{x(i-1)} v_{xi} \geq 0 \tag{50}$$

$v_{x(i-1)} > 0$, then t_{xk}^i belongs to decelerating intervals and the direction of F_x is along the negative direction of the x-axis; $v_{x(i-1)} \leq 0$, then t_{xk}^i belongs to accelerating intervals but the direction of F_x is along the positive direction of the x-axis. If $t_{xk}^i \neq 0, k \in (1, 2, ...N_x^i)$ and meets the following conditions.

$$|v_{x(i-1)}| > |v_{xi}|, \quad v_{x(i-1)} v_{xi} < 0 \tag{51}$$

$v_{x(i-1)} > 0$, then t_{xk}^i belongs to accelerating intervals and the direction of F_x is along the negative direction of the x-axis; $v_{x(i-1)} \leq 0$, then t_{xk}^i belongs to accelerating intervals but the direction of F_x is along the positive direction of the x-axis.

After the three types of time intervals in three axes in the ith arc are calculated, then the switching control laws can be given. Takeing the switching control law in the $x-axis$ as an example

$$S_x = \{x_{i-1}, v_{x(i-1)}; (t_{x1}^i, a_{x1}^i); ...(t_{xN_x^i}^i, a_{xN_x^i}^i)\} \tag{52}$$

$$a_{xk}^i = F_x \sum_{j=0}^{4} \lambda_{ji} (t_{xk}^i)^j. \quad k \in (1, 2, ...N_x^i) \tag{53}$$

V. Simulation results

Suppose that the height of target spacecraft is 400km in a circular orbit and the initial mass of the chaser and the propellant are $300kg$ and $100kg$. The size of thrusts are 360N, 240N and 320N in the x-axis, y-axis and in the z-axis, respectively. The mass-flow-rate of propellant of the chaser's thrusters are $20g/s$, $15g/s$ and $10g/s$ in the x-axis, y-axis and in the z-axis, respectively. Although η_x, η_y and η_z are variables, but they vary little during active collision avoidance maneuver, therefore, in order to facilitate simulation, these coefficients can be seen as constants: $\eta_x = \eta_y = \eta_z = 0.001$.

The initial relative position and the initial relative velocity of the chaser are $(500m, -500m, 500m)$ and $(-6m/s, 6m/s, -6m/s)$. The initial acceleration is zero and the expected docking velocity $V^* = 1m/s$. The minimum safe distance is $700m$ and the corresponding minimum time is $60s$. Based on the vision measurement, the radius of the first layer spherical security zone S_{C1} of the chaser $R_1 = 60m$ and the radius of the second layer spherical security zone $R_2 = 80m$. The distances from O_T to O_C at the first target maneuver position is $R_t^1 = 866m$. The longest line segments from all edge points of the target spacecraft to O_C at the first target maneuver position is $H_1O_C = 926.18m$. The angle between H_1O_C and O_TO_C is $\theta_1 = 3^o$. According to Eq.(18), the radius of the spherical security zone of the target spacecraft at the first target maneuver position is $r_1 = 80m$.

According to Eqs. (18),(19), there is a possibility of collision, the chaser should carry out active collision avoidance maneuver and the terminal target position is $(300m, 0m, 0m)$. And the specified trajectory is given as follow. The size of the cube is $\Delta_x = 200m, \Delta_y = 500m, \Delta_z = 500m$.

$$\begin{cases} 2.5 \times 10^{-5}(x - 500)^2 + 4 \times 10^{-6} y^2 = 1 \\ y + z = 0 \end{cases} \tag{54}$$

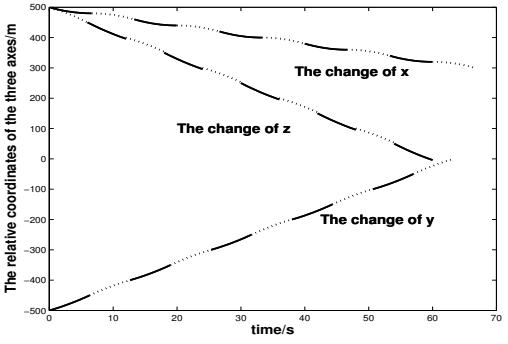

Figure 5: The change of x, y, z during active collision avoidance maneuver.

The results in Figure 5 show the change of x, y, z during active collision avoidance maneuver. x changes from 500m to 300m, y changes from -500m to 0m and z changes from 500m to 0m.

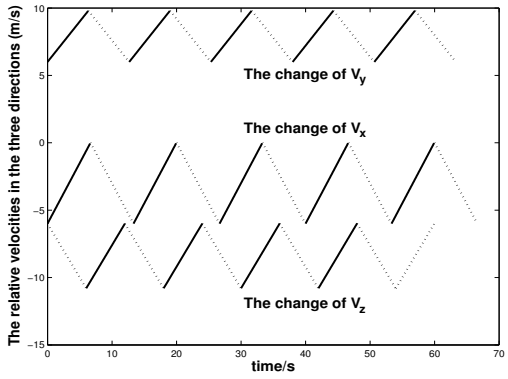

Figure 6: The change of V_x, V_y, V_z during active collision avoidance maneuver.

The results in Figure 6 show the change of V_x, V_y, V_z during active collision avoidance maneuver. V_x changes from -6m/s to 0m/s, V_y changes from 6m/s to 9.8m/s and V_z changes from -6m/s to -10.8m/s.

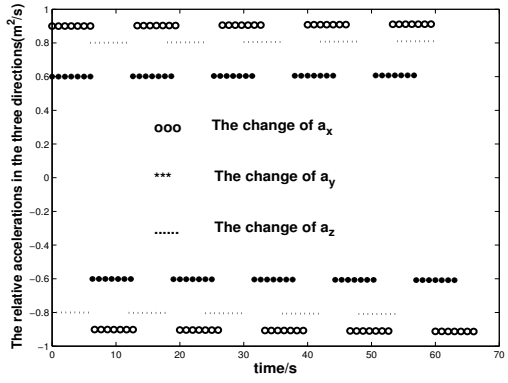

Figure 7: The change of a_x, a_y, a_z during active collision avoidance maneuver.

The results in Figure 7 show the change of a_x, a_y and a_z during active collision avoidance maneuver. a_x changes from $0.9m^2/s$ to $-0.9061m^2/s$. a_y changes from $0.6m^2/s$ to $0.6041m^2/s$. a_z changes from $-0.8m^2/s$ to $0.8049m^2/s$.

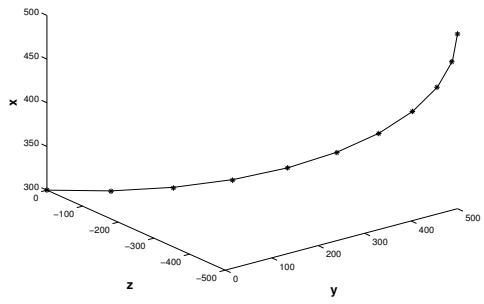

Figure 8: The trajectory of the chaser during active collision avoidance maneuver.

The result in Figure 8 shows the chaser maneuvers along the specified trajectory. Taking the switching control law in the $x-axis$ as an example:

$$S_x = \{500m; -6m/s; ([0, 6.33s], (0.9 \rightarrow 0.9007)m^2/s); \\ ...([60, 66.67s], (0.9054 \rightarrow -0.9061)m^2/s\} \quad (55)$$

VI. Conclusion

This paper deals with the active collision avoidance maneuver for the chaser moving along the specified trajectory, and presents a maneuver approach with constant thrust. Using the 3D stereo vision measurement, the position parameters of the target spacecraft are obtained. The target maneuver positions can be calculated through the equidistance interpolation method, and the working times of thrusters in three axes can be respectively computed by the time series analysis method. Furthermore, the acceleration sequences and the corresponding working time series can be employed to determine the switching control laws for the active collision avoidance maneuver. The simulation results show that the switching control laws can effectively guarantee the chaser moving along the specified trajectory.

References

[1] L. K. Newman, M. Duncan. Establishment and implementation of a close approach evaluation and avoidance process for Earth Observing System Missions. in: AAS/AIAA Astrodynamics Specialist Conference, Keystone, CO, AIAA-2006-6291.

[2] A. G. Richards, T. Schouwenaars, J. P. How, E. Feron. Spacecraft Trajectory Planning With Collision and Plume Avoidance Using Mixed Integer Linear Programming. AIAA Journal of Guidance, Control and Dynamics, vol. 25, pp.755-764, Aug 2002.

[3] I. Garcia and J. P. How. Trajectory Optimization for Satellite Reconfiguration Maneuvers with Position and Attitude Constraints. Proceedings of the IEEE American Control Conference, June 2005, pp.889-895

[4] C. Tomlin, I. Mitchell, R. Ghosh. Safety Verification of Conflict Resolution Maneuvers. IEEE Transactions on Intelligent Transportation Systems, vol 2., no 2., June 2001, p.110.

[5] S. Matsumoto, S. Dubowsky, S. Jacobsen, Y. Ohkami, Fly-by Approach and Guidance for Uncontrolled Rotating Satellite Capture. AIAA Guidance, Navigation, and Control Confrence, Austin, TX, Aug 11-14, 2003.

[6] Jacobsen, S., Lee, C., Zhu, C., and Dubowsky, S, Planning of Safe Kinematic Trajectories for Free Flying Robots Approaching an Uncontrolled Spinning Satellite, Proceedings of the ASME 27th Annual Biennial Mechanisms and Robotics Conference, American Society of Mechanical Engineers, Fairfield, NJ, Sept. 2002.

[7] Inalhan, G., Tillerson, M., and How, J., Relative Dynamics and Control of Spacecraft Formations in Eccentric Orbits, Journal of Guidance, Control and Dynamics, Vol. 25, No. 1, 2002.

[8] Richards, A., Schouwenaars, T., How, J., and Feron, E., Spacecraft trajectory planning with avoidance constraints using mixed-integer linear programming, Journal of Guidance, Control, and Dynamics, Vol. 25, No. 4, 2002, pp. 755-764.

[9] Tillerson, M., Inalhan, G., and How, J., Co-ordination and Control of Distributed Spacecraft Systems Using Convex Optimization Techniques, International Journal of Robust Nonlinear Control, Vol. 12, No. 1, 2002, pp. 207-242.

[10] Yamanaka, K. and Ankersen, F., New State Transition Matrix for Relative Motion on an Arbitrary Elliptical Orbit," Journal of Guidance, Control, and Dynamics, Vol. 25, No. 1, 2002, pp. 60-66.

[11] Gim, D. and Alfriend, K., State transition matrix of relative motion for the perturbed noncircular reference orbit, Journal of Guidance, Control, and Dynamics, Vol. 26, No. 6, 2003, pp. 956-971.